
Deep Ensembles for Graphs with Higher-order Dependencies

Steven J. Krieg

Lucy Family Institute for Data and Society
University of Notre Dame
Notre Dame, IN 46556
skrieg@nd.edu

William C. Burgis

Lucy Family Institute for Data and Society
University of Notre Dame
Notre Dame, IN 46556
wburgis@nd.edu

Patrick M. Soga

Lucy Family Institute for Data and Society
University of Notre Dame
Notre Dame, IN 46556
psoga@nd.edu

Nitesh V. Chawla*

Lucy Family Institute for Data and Society
University of Notre Dame
Notre Dame, IN 46556
nchawla@nd.edu

Abstract

Graph neural networks (GNNs) continue to achieve state-of-the-art performance on many graph learning tasks, but rely on the assumption that a given graph is a sufficient approximation of the true neighborhood structure. In the presence of higher-order sequential dependencies, we show that the tendency of traditional graph representations to underfit each node’s neighborhood causes existing GNNs to generalize poorly. To address this, we propose a novel **Deep Graph Ensemble** (DGE), which captures neighborhood variance by training an ensemble of GNNs on different neighborhood subspaces of the same node within a higher-order network structure. We show that DGE consistently outperforms existing GNNs on semisupervised and supervised tasks on four real-world data sets with known higher-order dependencies, even under a similar parameter budget. We demonstrate that learning diverse and accurate base classifiers is central to DGE’s success, and discuss the implications of these findings for future work on GNNs.

1 Introduction

The advent of graph neural networks (GNNs) has birthed many powerful machine learning solutions for graph problems. GNNs’ success lies in their ability to efficiently and expressively propagate information through neighborhoods [50, 44]. However, because the graph structure is the medium for sharing information, even the most powerful GNNs are limited by the representational quality of that structure. Most present work on GNNs assumes that a given graph is a sufficient approximation of the underlying system. However, a growing body of work has challenged this assumption by showing that traditional graphs often cannot capture the higher-order structure and dynamics that govern many real-world systems [25, 3, 29, 39, 2]. In the present work, we couple GNNs with a specific family of graphs, **higher-order networks** (HONs), which encode sequential dependencies (i.e., statistical patterns that cannot be accounted for in a first-order Markov model) in a graph structure [45]. HONs have been applied to the study of user behaviors [11], citation networks [30], human mobility and navigation patterns [36, 28], the spread of invasive species [45, 32], anomaly detection [33], disease progression [23], and many more [21, 28, 35, 25]. A traditional graph, which we call a **first-order network** (FON), represents a system by decomposing it into a set of pairwise edges, so the only

*Corresponding author.

way to infer polyadic interactions is via transitive paths over adjacent nodes. When higher-order dependencies are present, these Markovian paths do not reflect the true neighborhood and can produce many false positive interactions [25]. This means that critical information about the system is lost during graph construction, before learning even begins. As Figure 1 shows, this can have significant consequences for GNNs, which typically compute representations by recursively pooling features from each node’s neighborhood. If the neighborhood is a poor approximation of the true interactions in the system, GNN performance will suffer.

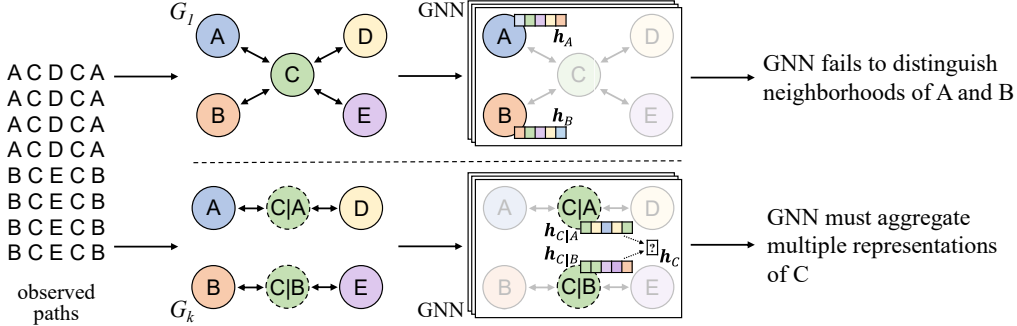


Figure 1: Toy examples of challenges faced by GNNs in modeling systems with higher-order dependencies. A FON (G_1 , top) underfits the dependencies in the observed paths. A HON (G_k , bottom) captures the true neighborhood by using multiple nodes to represent the same entity (C|A and C|B, indicated by a dashed outline, both represent C but in a different context), so representations h_u for each entity u are no longer straightforward to compute. Each color represent a unique entity.

In more general terms, when higher-order dependencies are present, a FON **underfits** the system [35]. To address this issue, Xu et al. introduced a model that allows one or more higher-order nodes to represent a single entity within a single-layer graph structure, while pruning nodes and paths that do not exhibit higher-order dependencies [45]. This HON paradigm has proven fruitful in a number of supervised and unsupervised settings [33, 31, 32, 23]. However, to our knowledge it has not yet been successfully used as input to a GNN. To enable GNNs to utilize the additional information encoded in HONs, we propose a novel **Deep Graph Ensemble** (DGE), which uses a set of independent GNNs to exploit variance in higher-order node neighborhoods and learn effective representations in graphs with higher-order dependencies. The **key contributions** of our work include:

1. We analyze the challenges that fundamentally limit the ability of existing GNNs to learn effective models of systems with higher-order dependencies.
2. We introduce the notion of neighborhood subspaces by showing that neighborhoods in a HON are analogous to feature subspaces of first-order neighborhoods. We then propose DGE to exploit the variance in these subspaces.
3. We experimentally compare DGE to eight state-of-the-art baselines on four real-world data sets with known higher-order dependencies, and show that, even with similar parameter budgets, DGE consistently outperforms all baselines on semisupervised (node classification) and supervised (link prediction) tasks.²
4. We demonstrate that DGE’s ability to train accurate and diverse classifiers is essential to its success, and show that training multiple GNNs with separate parameters is a consistent way to maximize both accuracy and diversity.

We first introduce relevant background for HONs, GNNs, and ensembles. Next, we present DGE and the justification for our design choices. We then present our experimental results. Finally, we discuss the limitations of our approach, other related work, and future directions.

2 Background and preliminaries

Higher-order networks Let $\mathcal{S} = \{S_1, S_2, \dots, S_n\}$ be a set of **observed paths**, where each $S_i = \langle s_1, s_2, \dots, s_m \rangle$ is a sequence of **entities**. Let also $\mathcal{A} = \bigcup \mathcal{S}$ be the set of entities across all sequences.

²Code available at <https://github.com/sjkrieg/dge>.

There is a large space of possible graph representations that we can construct to approximate \mathcal{S} . We consider two: a FON and a HON [45]. In a FON $G_1 = (V_1, E_1)$, the node set $V_1 = \mathcal{A}$ (or, more generally, the mapping $f : V_1 \rightarrow \mathcal{A}$ is bijective), and the edge set E_1 is the set of node pairs $(u, v) \in V_1 \times V_1$ that appear as adjacent elements in at least one sequence in \mathcal{S} .

In a HON $G_k = (V_k, E_k)$ with order $k > 1$, each **higher-order node** in V_k is a sequence of entities $u' = \langle a'_1, \dots, a'_{m-1}, a'_m \rangle$, where $a'_i \in V_1$ and $m \leq k$. We define a'_m as the **base node**, and in practice use the notation $u' = a'_m | a'_1, \dots, a'_{m-1}$ to emphasize that each higher-order node represents a base node whose current state is conditioned on a set of predecessors. Each node can have a different number of predecessors, and a node with $m > 1$ is only created if the conditional distribution of paths it encodes sufficiently reduces the entropy of the graph [33]. This means that $V_k \subseteq \mathcal{A}^k$; or, more generally, the mapping $f : V_k \rightarrow \mathcal{A}^k$ is injective but not necessarily bijective. We define $\Omega_u^k = \{u' \in V_k, a'_m = u\}$ as the **higher-order family** of u (including u itself), and call each $u' \in \Omega_u^k$ a **relative** of u . Like E_1 , the edge set E_k is the set of node pairs $(u, v) \in V_k \times V_k$ that are adjacent in at least one sequence in \mathcal{S} , but generalized to account for the fact that each node is a sequence rather than a single entity (prior work characterizes each edge as adjacent substrings in \mathcal{S} [22]). Edges are directed such that $(u, v) \neq (v, u)$ and weighted via $w_k : E_k \rightarrow \mathbb{R}_{\geq 0}$, where 0 indicates a missing edge. Because each node in V_k can represent one or more entities, each edge in E_k represents interactions between two or more entities while remaining a 2-tuple. This means that many graph operations can be easily applied to G_k , which preserves more information than G_1 with respect to \mathcal{S} but is less prone to overfitting than fixed-order models [45, 33, 22].

The term ‘‘higher-order’’ is also used in the literature to refer to the analysis of polyadic structures within graphs [4], as well GNNs that are able to distinguish these structures [27, 34]. These studies rely on the same assumptions as other GNNs about the sufficiency of the graph structure, and are therefore susceptible to the same limitations. Despite similarities in terminology, HONs are primarily concerned with the question of initial representation (i.e., how should the graph be constructed?) rather than downstream analysis, and thus address a fundamentally different problem [25]. HONs are also distinct from other formalisms like hypergraphs and simplicial complexes in that they encode sequential paths (via edge direction) and probability distributions (via edge weights), and are therefore used to represent different kinds of systems [3, 29, 39, 2].

Graph neural networks A generic GNN computes a hidden vector representation for a node u at timestamp t according to:

$$\mathbf{h}_u^{(t)} = \text{COMBINE}\left(\mathbf{h}_u^{(t-1)}, \text{AGGREGATE}\left(\{\mathbf{h}_v^{(t-1)}, v \in \mathcal{N}(u)\}\right)\right), \quad (1)$$

where $\mathcal{N}(u)$ is the neighborhood of u in a graph G . What typically distinguishes GNNs is how they define COMBINE and AGGREGATE, and how they represent $\mathcal{N}(u)$ [46, 50, 44]. By recursively pooling features via Eq. 1, GNNs implicitly construct higher-order neighborhoods across transitive paths. This assumption of transitivity is key to the success of GNNs, since it allows them to consider the influence of nonadjacent nodes [26, 9]. However, as we will demonstrate, when higher-order dependencies are present, this assumption leads GNNs that are trained on FONs to overfit and generalize poorly.

In this work, we do not reformulate Eq. 1 and are agnostic toward its particular implementation. We instead define a GNN as a function that takes u as input and returns either the final hidden representation $\mathbf{h}_u^{(t)}$, or, in a supervised setting, a vector of predicted label probabilities $\hat{\mathbf{y}}_u$:

$$\text{GNN}(u) = \mathbf{h}_u^{(t)} \quad \text{or} \quad \text{GNN}(u) = \hat{\mathbf{y}}_u. \quad (2)$$

We always assume that G contains initial node features $\{\mathbf{x}_u, \forall u \in V\}$ and that $\text{GNN}(\cdot)$ is parameterized by weights θ , but for simplicity we omit them from our notation.

Ensemble learning Many foundational ensembles combined shallow learners, each trained on different sample or feature subspaces, for significant performance improvements [5, 13, 14]. Ensembling deep models can also improve uncertainty estimation and robustness, often by using different weight initializations to exploit a neural network’s vast parameter space [17, 24, 15, 42]. Unfortunately, very few works have been published on ensembles of GNNs. A recent exception is Tang et al., who used data augmentation and knowledge distillation to teach a student GNN from an ensemble of teachers [38]. Before GNNs became popular, Yu et al. built an ensemble of k -nearest neighbor graphs

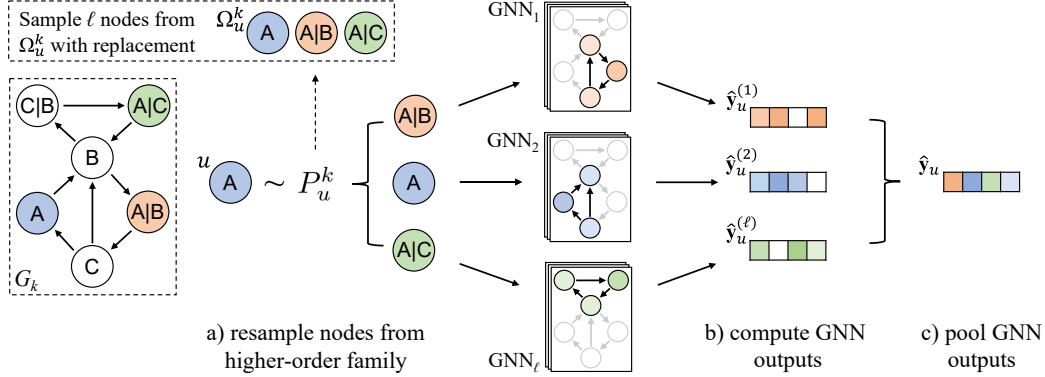


Figure 2: Overview of DGE. Given a HON G_k (edge weights not pictured), we compute outputs for each base node u by a) resampling relatives from u 's higher-order family Ω_u^k via a sampling distribution P_u^k , b) computing outputs for each sampled relative using independent GNN modules, and c) pooling the outputs. Relatives of A are colored to illustrate neighborhood differences.

from subspaces of high-dimensional features, but their approach does not generalize to settings in which only the graph structure is known [48]. In the present work, we lean on the prior success of ensembling techniques, especially the concept of using random subspaces to exploit variance in the feature space [18, 6], and the principle that ensembles are most potent when the predictions of their individual classifiers are accurate and diverse [13].

3 Deep graph ensembles for higher-order networks

In the following section, we first discuss the key challenges of learning on HONs and how ensemble learning techniques can address them. Second, we propose several methods for constructing an ensemble of GNNs. Figure 2 summarizes our proposed DGE framework.

3.1 Why deep graph ensembles?

There are a number of design challenges (CHs) we must address in order to realize the joint potential of GNNs and HONs. In a HON, entities are represented by a non-fixed number of higher-order nodes (**CH1**), each of which has a different neighborhood (**CH2**) and may be of varying importance (**CH3**) [45, 33, 31, 22]. One intuitive idea is to compute a representation for u by sampling neighbors from any of u 's relatives. However, this fails to address CH2 because a GNN would aggregate the samples without considering differences between relatives. Another intuitive idea is to compute representations for each relative separately, then merge them via a permutation-invariant function like an elementwise MEAN. But this does not address CH3, since all relatives would contribute equally to the final representation. Moreover, if we assume that all relatives in a higher-order family share the same (or similar) features, this solution introduces additional bias into the model process because the features associated with larger higher-order families will be overrepresented in the training data. To address these challenges, we first consider the relationship of u 's neighborhood to the neighborhoods of u 's relatives.

Theorem 1. *Let G_1 and G_k be a FON and HON, respectively, both constructed from the same input S . Let $\mathcal{N}_1(u)$ and $\mathcal{N}_k(u)$ denote the neighborhoods of any node u in G_1 and G_k , respectively. Let $\text{AGGREGATE}(\cdot)$ represent any symmetric neighborhood aggregation function. If $u \in V_1$ and $u' \in \Omega_u^k$, then $\text{AGGREGATE}(\mathcal{N}_k(u'))$ is a biased estimator of $\text{AGGREGATE}(\mathcal{N}_1(u))$.*

We prove Theorem 1 in Appendix A. The intuition is that u' only exists in G_k if the transition probabilities of a random walker are sufficiently different (measured via KL-divergence) from u in G_1 [33, 22]. These differences will be consequently be represented in the expectation of the features gathered by $\text{AGGREGATE}(\mathcal{N}_k(u'))$. Inspired by the idea of feature subspaces [18, 6], we call $\mathcal{N}_k(u')$ a **neighborhood subspace** of $\mathcal{N}_1(u)$. As long as the variance of $\mathcal{N}_k(u')$ is useful w.r.t. the learning task, we can use ensembling techniques to exploit its estimation error and improve GNN performance.

Specifically, we propose to train a set of GNNs $\{\text{GNN}_1, \text{GNN}_2, \dots, \text{GNN}_\ell\}$. Given a set of training nodes $D \subseteq V_1$, we generate bootstraps $\{D^{(1)}, D^{(2)}, \dots, D^{(\ell)}\}$ subject to the constraint that $|D^{(i)} \cap \Omega_u^k| = 1$ for all $u \in D$ and $i \leq \ell$ (i.e., each bootstrap contains exactly one relative of each training node). This constraint allows us to avoid the overrepresentation problem, address CH1 by sampling with replacement, and address CH2 by training each GNN_i on different neighborhood subspaces as represented in $D^{(i)}$. To solve CH3, we weight the sampling probability for each relative u' according to the normalized out-degree of its higher-order family:

$$P_u^k(u') = \frac{\text{OUTDEG}_k(u')}{\sum_{v' \in \Omega_u^k} \text{OUTDEG}_k(v')}, \quad (3)$$

where $u \in D$ and $\text{OUTDEG}_k(u')$ is the weighted out-degree of u' in G_k . Because weighted out-degree in G_k is the frequency with which u' appears in S (in-edges are rewired to preserve connectivity and thus in-degree is less stable [22]), it is a natural measure of the importance of u' in the graph.

When $D \subseteq E_1$ consists of node pairs for an edge task, we modify Eq. 3 slightly. Given an edge $(u, v) \in D$, we resample a pair of relatives (u', v') with probability according to the normalized weights of all edges between relatives of u and v :

$$P_{u,v}^k(u', v') = \frac{w_k(u', v')}{\sum_{(u'', v'') \in \Omega_u^k \times \Omega_v^k} (w_k(u'', v''))}, \quad (4)$$

subject to the constraint that $|D^{(i)} \cap (\Omega_u^k \times \Omega_v^k)| = 1$ for all $(u, v) \in D$ and $i \leq \ell$.

3.2 Training and inference

Let $D_u^{(i)}$ denote the relative of u that was sampled for the i^{th} bootstrap. We specifically consider a supervised or semisupervised setting, in which our goal is to compute a vector of class probabilities $\hat{\mathbf{y}}_u$ for each $u \in D$ such that some loss (w.r.t. the ground truth \mathbf{y}_u) is minimized. We propose three methods for computing $\hat{\mathbf{y}}_u$:

$$\hat{\mathbf{y}}_u = \sigma\left(\text{CONCAT}\left(\{\text{GNN}_i(D_u^{(i)}), \forall i \leq \ell\}\right)^\top \cdot \mathbf{W}\right) \quad \text{and} \quad \text{GNN}_i(u') = \mathbf{h}_{u'}^{(i,t)}, \quad (5a)$$

or

$$\hat{\mathbf{y}}_u = \sigma\left(\text{MEAN}\left(\{\text{GNN}_i(D_u^{(i)}), \forall i \leq \ell\}\right)^\top \cdot \mathbf{W}\right) \quad \text{and} \quad \text{GNN}_i(u') = \mathbf{h}_{u'}^{(i,t)}, \quad (5b)$$

or

$$\hat{\mathbf{y}}_u = \text{MEAN}\left(\{\text{GNN}_i(D_u^{(i)}), \forall i \leq \ell\}\right) \quad \text{and} \quad \text{GNN}_i(u') = \hat{\mathbf{y}}_{u'}^{(i)}, \quad (5c)$$

where σ is a non-linear activation, CONCAT is vector concatenation, MEAN is elementwise mean, \mathbf{x}^\top is the transpose of \mathbf{x} , $\mathbf{h}_{u'}^{(i,t)} \in \mathbb{R}^d$ represents the hidden state of node u' in the t^{th} (final) layer of GNN_i , and d is the number of hidden units (we assume this is fixed for all GNN_i). Using c to denote the number of classes, for Eq. 5a we have $\mathbf{W} \in \mathbb{R}^{d \times c}$, and for Eq. 5b we have $\mathbf{W} \in \mathbb{R}^{d \times c}$. We refer to Eq. 5a as **DGE-concat**, Eq. 5b as **DGE-pool**, and Eq. 5c as **DGE-bag**.

There are key differences among these formulations. Most notably, in DGE-concat and DGE-pool the outputs from each GNN are hidden states, which are pooled before computing the logits. This means that they can be trained in end-to-end fashion as a single neural network with parallel GNN modules. During a forward pass, the parameters of each GNN_i are only used to compute representations for nodes in the corresponding $D^{(i)}$. In DGE-bag, on the other hand, the outputs from each GNN are class probabilities, which means that all GNN are trained independently, and their outputs pooled later.

One important question is whether all GNN_i should share parameters. We evaluate this question experimentally, and use **DGE-concat***, **DGE-pool***, and **DGE-bag*** to denote implementations with shared parameters. For DGE-concat* and DGE-pool*, we adjusted our training procedure so that, during backpropagation, each parameter was updated once according to its contribution to the summed loss across all $D^{(i)}$. For DGE-bag*, this meant that GNN_i was essentially pretrained on $D^{(i-1)}$. We also considered one final variant, **DGE-batch***, which does not generate a fixed set of

Table 1: Key characteristics of graphs used in node classification and link prediction.

Name	$ S $	$ V_1 $	$ E_1 $	$ V_2 $	$ E_2 $	# classes	$\mathcal{H}(G_1)$	$\mathcal{H}(G_2)$
Air	17,146,666	416	13,735	7,461	236,806	10	0.351	0.288
T2D	829,672	908	314,352	5,462	367,530	16	0.099	0.099
Wiki	76,193	4,179	70,662	5,584	84,806	10	0.366	0.375
NY	3,799,715	4,079	1,873,279	9,568	1,957,602	4	0.323	0.336

bootstraps for training. Instead, we resample a new set of relatives for each minibatch (subject to the same constraints as each $D^{(i)}$). Then, during inference, we return to the procedure for DGE-bag: resample ℓ relatives for each node and compute their outputs via Eq. 5c. DGE-batch* therefore represents a traditional GNN that is trained with awareness of CH1 and CH3, and addresses CH2 in a manner similar to a READOUT function [44]. We considered DGE-batch* an important variant to evaluate because its performance illuminates the importance of using an ensemble instead of a single, more complex model to solve CH2 [1].

4 Experimental results and discussion

4.1 Experimental setup

Data sets We generated FONs and HONs with $k = 2$ (details in Appendix I) for four real-world data sets with known higher-order dependencies: flight itineraries for airline passengers in the United States (**Air**) [35], disease trajectories for type 2 diabetes patients in Indiana (**T2D**) [23], clickstreams of users playing the Wikipedia game (**Wiki**) [43], and readership trajectories for a large online magazine (**NY**) [41]. As summarized in Table 1, the graphs were relatively diverse with respect to size, density, differences between G_1 and G_2 , and average homophily \mathcal{H} (defined as the fraction of edges that connect nodes of the same class [51]). Additional details on these data are available in Appendix B. For models trained on G_1 we used identity features (i.e., one-hot encodings of the node indices) for each node. For models trained on G_2 , we used the same features as G_1 such that each $u' \in \Omega_u^2$ shared the same features as its base node u .

Tasks We evaluated DGE on node classification (semisupervised) and link prediction (supervised). For node classification, we used stratified 5-fold cross validation [37] and reported the mean micro F1-score. For link prediction, we generated training and testing sets by randomly sampling 10% of positive node pairs and an equal number of negative node pairs. In addition to hiding all edges (in both directions) between testing pairs, for experiments using G_2 we also hid all edges between any pair of nodes in the same higher-order families as each testing pair. We repeated each experiment five times and reported the mean area under the precision-recall curve (AUPRC) [47]. All experiments utilized the same training and testing splits.

Baselines We compared DGE to several baselines, including GCN [20], GAT [40], and GraphSAGE [16]. Two other GNNs that we considered particularly relevant were GraphSAINT [49] and GCNII [9]. GraphSAINT samples a different subgraph for each training iteration and has outperformed other GNNs on a number of tasks [19]. GCNII uses residual connections to address over-smoothing and enable deeper GNNs, which is particularly relevant given that the underfitting tendency of FONs becomes more problematic with longer paths [33, 22]. Other baselines included GIN, which introduced a sum aggregator to improve the discriminative ability of GNNs [46], and GATv2, which introduced a dynamic attention mechanism to address prior limitations of GAT [7]. We also evaluated HONEM, a matrix factorization method that is, to the best of our knowledge, the only supervised learning method that has been designed specifically for HONs [31].

Implementation details All baselines used G_1 as input (we also evaluated each baseline using G_2 as input, details are in Appendix D). We manually tuned each model (details in Appendix C). For DGE, unless noted otherwise, we fixed $\ell = 16$ and used the mean-pooling variant of GraphSAGE as the base GNN, since a) it performed reasonably well as a baseline on all four data sets, and b) its sample-and-aggregate procedure intuitively complements the relative sampling and pooling used by

Table 2: Node classification results (micro F1). Bold font indicates the best result for each data set.

Model	Air	T2D	Wiki	NY
GCN	0.818 \pm 0.03	0.480 \pm 0.02	0.643 \pm 0.01	0.796 \pm 0.01
GCNII	0.845 \pm 0.05	0.511 \pm 0.02	0.654 \pm 0.02	0.801 \pm 0.01
GAT	0.804 \pm 0.03	0.282 \pm 0.10	0.639 \pm 0.02	0.487 \pm 0.06
GATv2	0.838 \pm 0.03	0.292 \pm 0.07	0.643 \pm 0.03	0.495 \pm 0.05
GraphSAGE	0.781 \pm 0.04	0.654 \pm 0.04	0.625 \pm 0.02	0.828 \pm 0.02
GIN	0.745 \pm 0.02	0.673 \pm 0.04	0.636 \pm 0.02	0.826 \pm 0.02
GraphSAINT	0.802 \pm 0.02	0.600 \pm 0.07	0.664 \pm 0.01	0.821 \pm 0.02
HONEM	0.805 \pm 0.04	0.566 \pm 0.02	0.588 \pm 0.01	0.728 \pm 0.02
DGE-concat	0.825 \pm 0.04	0.501 \pm 0.06	0.615 \pm 0.02	0.790 \pm 0.02
DGE-concat*	0.810 \pm 0.04	0.439 \pm 0.03	0.577 \pm 0.02	0.761 \pm 0.02
DGE-pool	0.839 \pm 0.03	0.735 \pm 0.03	0.671 \pm 0.01	0.860 \pm 0.01
DGE-pool*	0.865 \pm 0.02	0.555 \pm 0.07	0.599 \pm 0.04	0.775 \pm 0.01
DGE-bag	0.856 \pm 0.02	0.770 \pm 0.04	0.681 \pm 0.00	0.871 \pm 0.01
DGE-bag*	0.766 \pm 0.04	0.719 \pm 0.04	0.644 \pm 0.02	0.841 \pm 0.02
DGE-batch*	0.764 \pm 0.03	0.646 \pm 0.01	0.623 \pm 0.01	0.818 \pm 0.01

* shared parameters

Table 3: Link prediction results (AUPRC). Bold font indicates the best result for each data set.

Model	Air	T2D	Wiki	NY
GCN	0.794 \pm 0.01	0.793 \pm 0.00	0.741 \pm 0.01	0.742 \pm 0.00
GCNII	0.806 \pm 0.01	0.754 \pm 0.01	0.781 \pm 0.01	0.750 \pm 0.00
GAT	0.786 \pm 0.01	0.698 \pm 0.02	0.797 \pm 0.01	0.644 \pm 0.00
GATv2	0.771 \pm 0.01	0.701 \pm 0.01	0.794 \pm 0.01	0.645 \pm 0.01
GraphSAGE	0.782 \pm 0.02	0.713 \pm 0.01	0.758 \pm 0.01	0.717 \pm 0.00
GIN	0.800 \pm 0.01	0.704 \pm 0.00	0.745 \pm 0.01	0.717 \pm 0.00
GraphSAINT	0.718 \pm 0.01	0.797 \pm 0.00	0.688 \pm 0.01	0.750 \pm 0.00
HONEM	0.697 \pm 0.02	0.818 \pm 0.00	0.589 \pm 0.01	0.769 \pm 0.00
DGE-concat	0.886 \pm 0.01	0.815 \pm 0.01	0.774 \pm 0.01	0.802 \pm 0.00
DGE-concat*	0.856 \pm 0.01	0.779 \pm 0.01	0.712 \pm 0.02	0.769 \pm 0.01
DGE-pool	0.851 \pm 0.02	0.920 \pm 0.00	0.838 \pm 0.03	0.913 \pm 0.00
DGE-pool*	0.845 \pm 0.01	0.901 \pm 0.00	0.802 \pm 0.06	0.898 \pm 0.00
DGE-bag	0.887 \pm 0.00	0.907 \pm 0.00	0.876 \pm 0.01	0.921 \pm 0.00
DGE-bag*	0.862 \pm 0.02	0.894 \pm 0.00	0.856 \pm 0.00	0.916 \pm 0.00
DGE-batch*	0.853 \pm 0.03	0.871 \pm 0.01	0.830 \pm 0.01	0.887 \pm 0.00

* shared parameters

DGE. We used Python 3.7.3 and Tensorflow 2.4.1 for all experiments, and utilized Stellargraph 1.2.1 [12] for all neighborhood sampling functions and the implementation of DGE.

4.2 Experimental results

Node classification and link prediction On the node classification task, DGE-bag outperformed all other methods on 3 data sets (Table 2). DGE-pool performed marginally worse than DGE-bag in all cases, but DGE-concat did not generalize well and performed poorly. Sharing parameters typically reduced performance for each DGE variant, excepting DGE-pool* on Air. We discuss this observation in Section 4.3. Some baselines were competitive: GCNII and GATv2 performed well on Air, and GCNII and GraphSAINT performed well on Wiki. However, on NY and especially T2D, DGE-bag outperformed all baselines by a significant margin. The full-batch models struggled on T2D, perhaps due to its combination of high density, meaning that there are many transitive paths, and low homophily, which is a known obstacle for many GNNs [51] (see discussion in Appendix H). The link prediction results tell a similar story (Table 3), but the margin by which

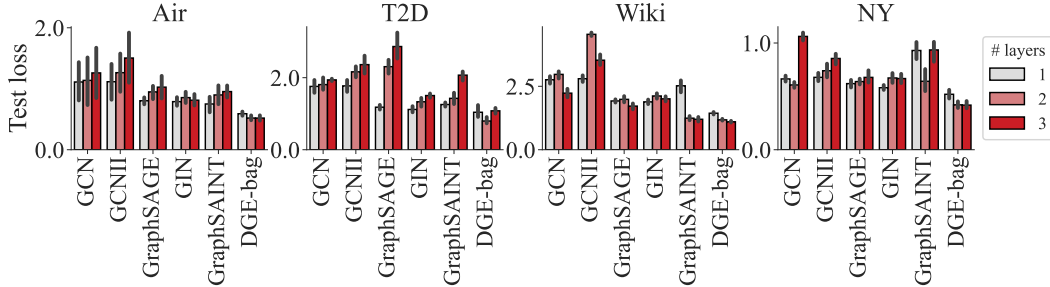


Figure 3: Test loss (node classification) by model depth. Error bars represent standard deviation.

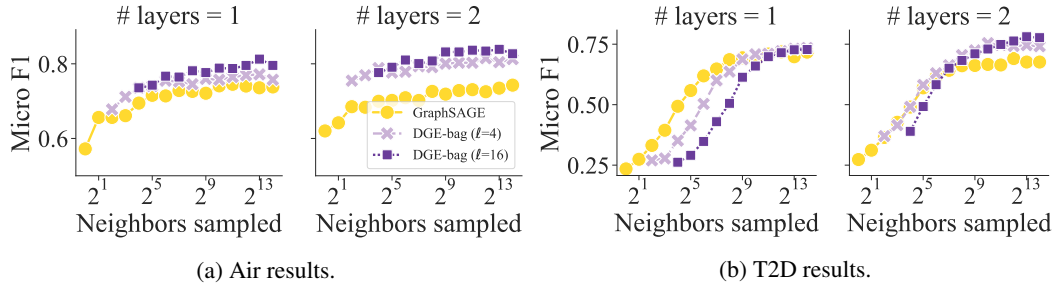


Figure 4: Node classification results as a function of the number of neighbors sampled. Each model was allotted the same sampling budget (e.g., for DGE ($\ell = 4$), 2^2 on the x-axis means that each base learner only sampled 1 neighbor) and 2,048 hidden units (e.g., each base learner for DGE ($\ell = 4$) had 512 hidden units). Each point represents one 5-fold cross validation experiment.

DGE-bag outperformed baselines was even more significant. DGE-concat was competitive on Air only, and DGE-pool produced the best result on T2D, but DGE-bag was strong across all data sets. The shared parameter variants of DGE performed better relative to baselines, but were still consistently worse than their counterparts. We did not find the performance of any baselines to be noteworthy. Because of its strong performance, we focus the remainder of our analysis on DGE-bag.

Model depth For all baselines, increasing the number of layers (model depth) typically increased generalization error (Figure 3). We excluded GAT and GATv2, which produced extremely high test error with 2 and 3 layers, likely because they compute attention weights (instead of edge weights) so were more susceptible to overfitting on insignificant edges. For DGE-bag, the test loss decreased with increased model depth in all but one case (layer 3 on T2D). These results support the findings of prior work that transitively inferring paths in a FON cannot account for higher-order dependencies [25], and our hypothesis that GNNs trained on G_1 will overfit on non-existent paths. The exception to this pattern was Wiki, on which almost all models performed best with 3 layers (GCNII was the only model we tested with more than 3 layers, but it performed best with only a single layer). This difference can perhaps be explained by the observation that Wiki was built from the smallest set of observed paths and was the sparsest graph, meaning that the likelihood of sampling a false positive path is relatively low due to smaller average neighborhood sizes. But even in this case, DGE-bag still produced the lowest test error at all depths.

Model width We also compared DGE-bag to GraphSAGE (the base GNN) while controlling for the total number of neighborhood samples and parameters (Figure 4). GraphSAGE used approximately 800k and 5.1m parameters for Air with one and two layers, respectively, and 1.9m and 6.1m for T2D with one and two layers, respectively. DGE-bag used the same number of parameters with a single layer, but fewer with two layers (about 1.3m and 2.3m for Air and T2D, respectively, with $\ell = 16$) since there were fewer dense connections between the first and second layers. On Air, DGE-bag outperformed GraphSAGE, even with very few samples. On T2D, all models required a higher sampling budget in order to perform well. With only a single layer, DGE-bag demonstrated no advantage; however, at the second layer, DGE-bag’s performance improved while GraphSAGE began to overfit. The results for Wiki and NY were similar to Air and T2D, respectively, so we have excluded them for brevity.

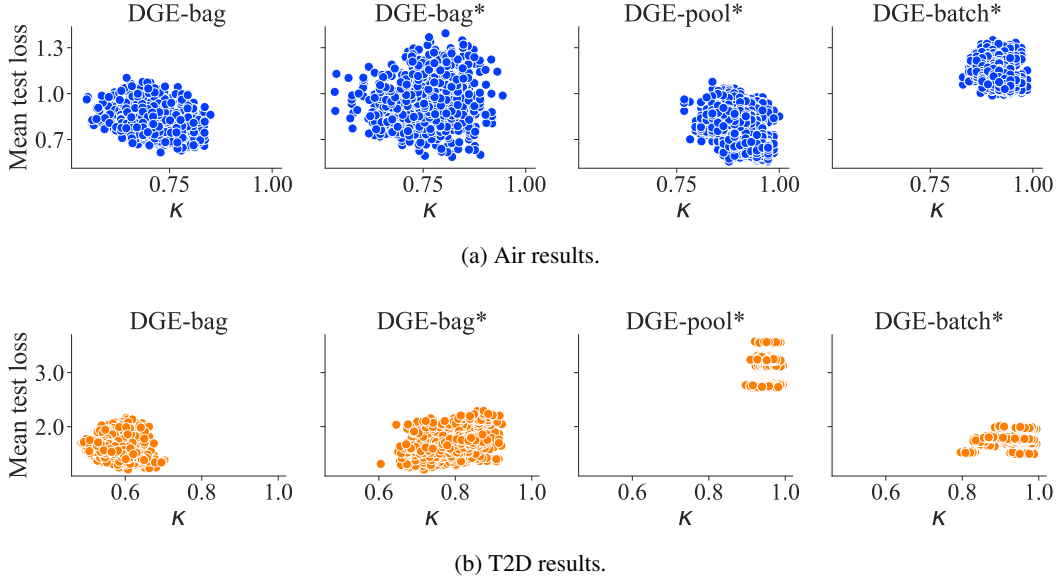


Figure 5: Mean node classification loss of each pair of classifiers, plotted as a function of Cohen’s kappa (lower values indicate lower agreement). Each point represents one pairwise comparison between the 16 classifiers in each of the 5 testing folds. All plots contain the same number of points.

One shortcoming of DGE is that the minimum number of parameters it requires to perform adequately is higher than for the baselines. The experiments in Figure 4 allowed for 2,048 hidden units (per layer), but GraphSAGE produced approximately the same results with only 256 hidden units. Other baselines also only required 128 or 256 hidden units. In our experiments, the performance of DGE-bag on two of the four data sets deteriorated when we allowed fewer than 128 hidden units per base learner (details in Appendix F). This means that DGE has higher minimum requirements but benefits significantly more than baselines from an increased parameter budget.

4.3 Ensemble diversity and parameter sharing

The variants of DGE that used separate parameters generally performed best. To understand this result, we draw from prior work on ensembles, which has established that ensembles most potent when the individual classifiers have low error and high disagreement [13]. Figure 5 visualizes DGE-bag and three of the shared parameter variants (using the same parameter budget described in Section 4.2 for all models) via Cohen’s kappa [13]. On both Air and T2D, DGE-bag consistently produced classifiers that both diverse and accurate. The shared parameter variants often produced classifiers that were either diverse or accurate, but not both. The results for Wiki and NY were similar to Air and T2D, respectively (Appendix D). These observations reflect classification performance (Table 2) and support a number of important conclusions. First, the high disagreement for DGE-bag demonstrates that our notion of neighborhood subspaces successfully introduced variance into the model. Second, the low mean error for DGE-bag demonstrates that ensembling GNNs with separate parameters effectively captured and exploited this variance. Third, sharing parameters (the equivalent of using a single, more complex model) did not achieve the same effect. DGE-pool* outperformed DGE-bag on Air because the classifier error was low enough to make up for the lack of disagreement. This may be because Air had large higher-order families, so each bootstrap was less representative of the true neighborhood. Future work, including generalizing DGE to other types of graphs, will require improving diversity and accuracy without sacrificing one for the other.

5 Limitations, other related work, and future directions

DGE’s empirical success has implications for multiple research areas. Most broadly, we suggest that ensembling techniques for GNNs have been underexplored. The variance DGE utilizes is not random, however, which complicates generalization to other problems. Our present work is also limited in that it relies on the HON to supply the neighborhood variance, which is in turn limited to

representing sequential data. Scalability and efficiency is another limitation our work shares with both deep ensembles and GNNs (see Appendix G for details on convergence times).

Our results also suggest that the task of designing accurate graph representations like HONs is essential and has been previously overshadowed by downstream learning algorithms. Recent work on higher-order models has made progress toward this end [25, 3, 29, 39, 2], but much work remains to generalize these models and the types of dependencies they can represent. One area we consider promising for future work is graph structure learning. At present, HONs are constructed in unsupervised fashion, but future work could overcome this limitation by inferring the graph structure that best solves the given task [8, 10]. Unfortunately, most standard data sets for GNN tasks are pre-constructed graphs, meaning that any higher-order dependencies (sequential or otherwise) have already been lost before learning begins. By integrating graph construction into the learning process and continuing to develop more powerful GNNs, we will increase our capacity to model higher-order relationships and expand the frontier of machine learning on graphs.

References

- [1] T. Abe, E. K. Buchanan, G. Pleiss, R. Zemel, and J. P. Cunningham. Deep ensembles work, but are they necessary? *arXiv preprint arXiv:2202.06985*, 2022.
- [2] F. Battiston, E. Amico, A. Barrat, G. Bianconi, G. Ferraz de Arruda, B. Franceschiello, I. Iacopini, S. Kéfi, V. Latora, Y. Moreno, et al. The physics of higher-order interactions in complex systems. *Nature Physics*, 17(10):1093–1098, 2021.
- [3] F. Battiston, G. Cencetti, I. Iacopini, V. Latora, M. Lucas, A. Patania, J.-G. Young, and G. Petri. Networks beyond pairwise interactions: structure and dynamics. *Physics Reports*, 874:1–92, 2020.
- [4] A. R. Benson, D. F. Gleich, and J. Leskovec. Higher-order organization of complex networks. *Science*, 353(6295):163–166, 2016.
- [5] L. Breiman. Bagging predictors. *Machine learning*, 24(2):123–140, 1996.
- [6] L. Breiman. Random forests. *Machine learning*, 45(1):5–32, 2001.
- [7] S. Brody, U. Alon, and E. Yahav. How attentive are graph attention networks? *International Conference on Learning Representations*, 2022.
- [8] I. Brugere and T. Y. Berger-Wolf. Inferring network structure from data. *arXiv preprint arXiv:2004.02046*, 2020.
- [9] M. Chen, Z. Wei, Z. Huang, B. Ding, and Y. Li. Simple and deep graph convolutional networks. In *International Conference on Machine Learning*, pages 1725–1735. PMLR, 2020.
- [10] Y. Chen and L. Wu. Graph neural networks: Graph structure learning. In *Graph Neural Networks: Foundations, Frontiers, and Applications*, pages 297–321. Springer, 2022.
- [11] F. Chierichetti, R. Kumar, P. Raghavan, and T. Sarlos. Are web users really markovian? In *Proceedings of the 21st international conference on World Wide Web*, pages 609–618, 2012.
- [12] C. Data61. Stellargraph machine learning library. <https://github.com/stellargraph/stellargraph>, 2018.
- [13] T. G. Dietterich. Ensemble methods in machine learning. In *International workshop on multiple classifier systems*, pages 1–15. Springer, 2000.
- [14] T. G. Dietterich. An experimental comparison of three methods for constructing ensembles of decision trees: Bagging, boosting, and randomization. *Machine learning*, 40(2):139–157, 2000.
- [15] S. Fort, H. Hu, and B. Lakshminarayanan. Deep ensembles: A loss landscape perspective. *arXiv preprint arXiv:1912.02757*, 2019.
- [16] W. Hamilton, Z. Ying, and J. Leskovec. Inductive representation learning on large graphs. *Advances in neural information processing systems*, 30, 2017.

- [17] L. K. Hansen and P. Salamon. Neural network ensembles. *IEEE transactions on pattern analysis and machine intelligence*, 12(10):993–1001, 1990.
- [18] T. K. Ho. The random subspace method for constructing decision forests. *IEEE transactions on pattern analysis and machine intelligence*, 20(8):832–844, 1998.
- [19] W. Hu, M. Fey, M. Zitnik, Y. Dong, H. Ren, B. Liu, M. Catasta, and J. Leskovec. Open graph benchmark: Datasets for machine learning on graphs. *Advances in neural information processing systems*, 33:22118–22133, 2020.
- [20] T. N. Kipf and M. Welling. Semi-supervised classification with graph convolutional networks. In *International Conference on Learning Representations (ICLR)*, 2017.
- [21] A. Koher, H. H. Lentz, P. Hövel, and I. M. Sokolov. Infections on temporal networks—a matrix-based approach. *PloS one*, 11(4):e0151209, 2016.
- [22] S. J. Krieg, P. M. Kogge, and N. V. Chawla. Growhon: A scalable algorithm for growing higher-order networks of sequences. In *International Conference on Complex Networks and Their Applications*, pages 485–496. Springer, 2020.
- [23] S. J. Krieg, D. H. Robertson, M. P. Pradhan, and N. V. Chawla. Higher-order networks of diabetes comorbidities: Disease trajectories that matter. In *2020 IEEE International Conference on Healthcare Informatics (ICHI)*, pages 1–11. IEEE, 2020.
- [24] B. Lakshminarayanan, A. Pritzel, and C. Blundell. Simple and scalable predictive uncertainty estimation using deep ensembles. *Advances in neural information processing systems*, 30, 2017.
- [25] R. Lambiotte, M. Rosvall, and I. Scholtes. From networks to optimal higher-order models of complex systems. *Nature physics*, 15(4):313–320, 2019.
- [26] Q. Li, Z. Han, and X.-M. Wu. Deeper insights into graph convolutional networks for semi-supervised learning. In *Thirty-Second AAAI conference on artificial intelligence*, 2018.
- [27] C. Morris, M. Ritzert, M. Fey, W. L. Hamilton, J. E. Lenssen, G. Rattan, and M. Grohe. Weisfeiler and leman go neural: Higher-order graph neural networks. In *Proceedings of the AAAI conference on artificial intelligence*, volume 33, pages 4602–4609, 2019.
- [28] T. P. Peixoto and M. Rosvall. Modelling sequences and temporal networks with dynamic community structures. *Nature communications*, 8(1):582, 2017.
- [29] M. A. Porter. Nonlinearity+ networks: A 2020 vision. In *Emerging Frontiers in Nonlinear Science*, pages 131–159. Springer, 2020.
- [30] M. Rosvall, A. V. Esquivel, A. Lancichinetti, J. D. West, and R. Lambiotte. Memory in network flows and its effects on spreading dynamics and community detection. *Nature communications*, 5:4630, 2014.
- [31] M. Saebi, G. L. Ciampaglia, L. M. Kaplan, and N. V. Chawla. Honem: learning embedding for higher order networks. *Big Data*, 8(4):255–269, 2020.
- [32] M. Saebi, J. Xu, S. R. Curasi, E. K. Grey, N. V. Chawla, and D. M. Lodge. Network analysis of ballast-mediated species transfer reveals important introduction and dispersal patterns in the arctic. *Scientific reports*, 10(1):1–15, 2020.
- [33] M. Saebi, J. Xu, L. M. Kaplan, B. Ribeiro, and N. V. Chawla. Efficient modeling of higher-order dependencies in networks: from algorithm to application for anomaly detection. *EPJ Data Science*, 9(1):15, 2020.
- [34] T. Schnake, O. Eberle, J. Lederer, S. Nakajima, K. T. Schutt, K.-R. Mueller, and G. Montavon. Higher-order explanations of graph neural networks via relevant walks. *IEEE Transactions on Pattern Analysis & Machine Intelligence*, pages 1–1, 2021.
- [35] I. Scholtes. When is a network a network? In *Proceedings of the 23rd ACM SIGKDD International Conference on Knowledge Discovery and Data Mining*, pages 1037–1046. ACM, 2017.

- [36] I. Scholtes et al. Causality-driven slow-down and speed-up of diffusion in non-markovian temporal networks. *Nature communications*, 5:5024, 2014.
- [37] O. Shchur, M. Mumme, A. Bojchevski, and S. Günnemann. Pitfalls of graph neural network evaluation. *arXiv preprint arXiv:1811.05868*, 2018.
- [38] H. Tang, X. Liang, B. Wu, Z. Guan, Y. Guo, and X. Zheng. Graph ensemble networks for semi-supervised embedding learning. In *International Conference on Knowledge Science, Engineering and Management*, pages 408–420. Springer, 2021.
- [39] L. Torres, A. S. Blevins, D. Bassett, and T. Eliassi-Rad. The why, how, and when of representations for complex systems. *SIAM Review*, 63(3):435–485, 2021.
- [40] P. Veličković, G. Cucurull, A. Casanova, A. Romero, P. Lio, and Y. Bengio. Graph attention networks. *International Conference on Learning Representations*, 2018.
- [41] D. Wang, M. Jiang, M. Syed, O. Conway, V. Juneja, S. Subramanian, and N. V. Chawla. Calendar graph neural networks for modeling time structures in spatiotemporal user behaviors. In *Proceedings of the 26th ACM SIGKDD international conference on knowledge discovery & data mining*, pages 2581–2589, 2020.
- [42] A. Wasay and S. Idreos. More or less: When and how to build convolutional neural network ensembles. In *International Conference on Learning Representations*, 2020.
- [43] R. West, J. Pineau, and D. Precup. Wikispeedia: An online game for inferring semantic distances between concepts. In *Twenty-First International Joint Conference on Artificial Intelligence*, 2009.
- [44] Z. Wu, S. Pan, F. Chen, G. Long, C. Zhang, and S. Y. Philip. A comprehensive survey on graph neural networks. *IEEE transactions on neural networks and learning systems*, 32(1):4–24, 2020.
- [45] J. Xu, T. L. Wickramaratne, and N. V. Chawla. Representing higher-order dependencies in networks. *Science advances*, 2(5):e1600028, 2016.
- [46] K. Xu, W. Hu, J. Leskovec, and S. Jegelka. How powerful are graph neural networks? In *International Conference on Learning Representations*, 2019.
- [47] Y. Yang, R. N. Lichtenwalter, and N. V. Chawla. Evaluating link prediction methods. *Knowledge and Information Systems*, 45(3):751–782, 2015.
- [48] G. Yu, G. Zhang, Z. Yu, C. Domeniconi, J. You, and G. Han. Semi-supervised ensemble classification in subspaces. *Applied Soft Computing*, 12(5):1511–1522, 2012.
- [49] H. Zeng, H. Zhou, A. Srivastava, R. Kannan, and V. Prasanna. Graphsaint: Graph sampling based inductive learning method. *International Conference on Learning Representations*, 2020.
- [50] J. Zhou, G. Cui, S. Hu, Z. Zhang, C. Yang, Z. Liu, L. Wang, C. Li, and M. Sun. Graph neural networks: A review of methods and applications. *AI Open*, 1:57–81, 2020.
- [51] J. Zhu, Y. Yan, L. Zhao, M. Heimann, L. Akoglu, and D. Koutra. Beyond homophily in graph neural networks: Current limitations and effective designs. *Advances in Neural Information Processing Systems*, 33:7793–7804, 2020.

Appendices

A Proof of Theorem 1

Preliminaries Without loss of generality, in this section we treat the neighborhood $\mathcal{N}_k(u')$ in a graph G_k for $k \geq 1$ as only the out-neighbors of u' (i.e. $\mathcal{N}_k(u') = \{v \in V_k, w_k(u', v) > 0\}$) and ignore in-edges. Given a node $u \in V_1$ and one of its relatives $u' \in \Omega_u^k$, we first define the Kullback-Leibler divergence of $\mathcal{N}_k(u')$ with respect to $\mathcal{N}_1(u)$:

$$D_{KL}(\mathcal{N}_k(u') \parallel \mathcal{N}_1(u)) = \sum_{v \in \mathcal{N}_1(u)} \pi_1(u \rightarrow v) \log_2 \frac{\pi_1(u \rightarrow v)}{\pi_k(u' \rightarrow v)}, \quad (6)$$

where $\pi_k(u' \rightarrow v) = \frac{w_k(u', v)}{\text{outdeg}_k(u')}$ is the probability that a random walker defined on G_k would step from u' to v . Our notation throughout this section assumes that $v \in \mathcal{N}_1(u)$ and $v \in \mathcal{N}_k(u')$; however, a relative $v' \in \Omega_v^k$ often replaces v in $\mathcal{N}_k(u')$. For example, in Figure 2, A|C is substituted for A in the neighborhood of C|B, but the edge (C|B, A|C) still fundamentally represents a step from C to A [22].

Following Saebi et al.[33], we constructed G_k such that $u' \in V_k$ iff the following inequality holds:

$$D_{KL}(\mathcal{N}_k(u') \parallel \mathcal{N}_1(u)) > \frac{m}{\log_2(1 + \text{freq}(u'))}, \quad (7)$$

where $m > 1$ is length of the sequence encoded by u' (see Section 2) and $\text{freq}(u') \geq 1$ is the number of times u' occurs in one of the observed paths in \mathcal{S} .

Lemma 1. *If $u \in V_1$ and $u' \in \Omega_u^k$, then there exists at least one node $v \in \mathcal{N}_1(u)$ such that $\pi_1(u \rightarrow v) \neq \pi_k(u' \rightarrow v)$.*

Proof. If $u' \in \Omega_u^k$, then $D_{KL}(\mathcal{N}_k(u') \parallel \mathcal{N}_1(u)) > 0$. This is because $\text{freq}(u') \geq 1$, so $\log_2(1 + \text{freq}(u')) \geq 1$ and the right side of Eq. 7 cannot be negative. If $D_{KL}(\mathcal{N}_k(u') \parallel \mathcal{N}_1(u)) = 0$, then the inequality in Eq. 7 cannot hold, so $u' \notin V_k$ and, consequently, $u' \notin \Omega_u^k$. Additionally, if $\pi_1(u \rightarrow v) = \pi_k(u' \rightarrow v)$ for all $v \in \mathcal{N}_1(u)$, then by Gibbs' inequality we have $D_{KL}(\mathcal{N}_k(u') \parallel \mathcal{N}_1(u)) = 0$. Therefore, since $u' \in \Omega_u^k$, there must exist at least one node $v \in \mathcal{N}_1(u)$ such that $\pi_1(u \rightarrow v) \neq \pi_k(u' \rightarrow v)$. \square

We now restate and prove Theorem 1.

Theorem 1. *Let G_1 and G_k be a FON and HON, respectively, both constructed from the same input \mathcal{S} . Let $\mathcal{N}_1(u)$ and $\mathcal{N}_k(u)$ denote the neighborhoods of any node u in G_1 and G_k , respectively. Let $\text{AGGREGATE}(\cdot)$ represent any symmetric neighborhood aggregation function. If $u \in V_1$ and $u' \in \Omega_u^k$, then $\text{AGGREGATE}(\mathcal{N}_k(u'))$ is a biased estimator of $\text{AGGREGATE}(\mathcal{N}_1(u))$.*

Proof. Without loss of generality, we consider the case in which AGGREGATE operates on a sample of neighbors (i.e., GraphSAGE [16]). Let $\mathcal{V} \sim \mathcal{N}_k(u')$ denote a random sample drawn from $\mathcal{N}_k(u')$. Assuming we weight the sampling distribution according to edge weights, we can write the probability of sampling any node v as

$$p(\mathcal{V} = v) = \frac{w_k(u', v)}{\text{outdeg}_k(u')} = \pi_k(u' \rightarrow v), \quad (8)$$

where $w_k(u', v)$ is the weight of edge (u', v) in G_k (Section 2) and $\text{outdeg}_k(u')$ is the weighted out-degree of u' in G_k . If we say that each $u \in V_k$ is represented by a real-valued feature vector $\mathbf{x}_u^k = [x_{u,1}^{(k)}, x_{u,2}^{(k)}, \dots, x_{u,d}^{(k)}]$, then, for a single sample drawn from $\mathcal{N}_k(u')$, we can formulate the expected value for each vector as follows:

$$\mathbb{E}_{\mathcal{V} \sim \mathcal{N}_k(u')} [\mathbf{x}_{\mathcal{V}}^k] = p(\mathcal{V} = v) \mathbf{x}_v^k. \quad (9)$$

If we combine these feature vectors for each of the n nodes in V_k , then we can represent the full expectation of \mathcal{V} as a neighborhood matrix

$$\begin{aligned}\mathbb{E}_{\mathcal{V} \sim \mathcal{N}_k(u')}[\mathcal{V}] &= \begin{bmatrix} p(\mathcal{V} = 1) \mathbf{x}_1^k \\ p(\mathcal{V} = 2) \mathbf{x}_2^k \\ \vdots \\ p(\mathcal{V} = n) \mathbf{x}_n^k \end{bmatrix} \\ &= \begin{bmatrix} p(\mathcal{V} = 1) x_{1,1}^{(k)} & p(\mathcal{V} = 1) x_{1,2}^{(k)} & \dots & p(\mathcal{V} = 1) x_{1,d}^{(k)} \\ p(\mathcal{V} = 2) x_{2,1}^{(k)} & p(\mathcal{V} = 2) x_{2,2}^{(k)} & \dots & p(\mathcal{V} = 2) x_{2,d}^{(k)} \\ \vdots & \vdots & \ddots & \vdots \\ p(\mathcal{V} = n) x_{n,1}^{(k)} & p(\mathcal{V} = n) x_{n,2}^{(k)} & \dots & p(\mathcal{V} = n) x_{n,d}^{(k)} \end{bmatrix}.\end{aligned}$$

We can simplify our notation by assuming the initial feature vectors are identity features (i.e., one-hot encodings of the node indices) defined on the base nodes, i.e., for features of nodes in V_1 , we have $x_{u,j}^{(1)} = \delta_{uj}$ for all $u, j \leq d = n$, where δ is the Kronecker delta. For the features of nodes in V_k , we assume that each $u' \in \Omega_u^k$ uses the same features as its base node, i.e., $x_{u',j}^{(k)} = \delta_{uj}$. Substituting these values in the above matrix gives

$$\mathbb{E}_{\mathcal{V} \sim \mathcal{N}_k(u')}[\mathcal{V}] = \begin{bmatrix} p(\mathcal{V} = 1) & 0 & \dots & 0 \\ 0 & p(\mathcal{V} = 2) & \dots & 0 \\ \vdots & \vdots & \ddots & \vdots \\ 0 & 0 & \dots & p(\mathcal{V} = n) \end{bmatrix}.$$

Without loss of generality, let AGGREGATE be the feature-wise MEAN of N samples drawn from $\mathcal{N}_k(u')$. We can then represent the expectation of AGGREGATE as

$$\begin{aligned}\mathbb{E}_{\mathcal{V} \sim \mathcal{N}_k(u')}[\text{AGGREGATE}(\mathcal{V})] &= \begin{bmatrix} \frac{1}{N} \\ \frac{1}{N} \\ \vdots \\ \frac{1}{N} \end{bmatrix} \begin{bmatrix} Np(\mathcal{V} = 1) & 0 & \dots & 0 \\ 0 & Np(\mathcal{V} = 2) & \dots & 0 \\ \vdots & \vdots & \ddots & \vdots \\ 0 & 0 & \dots & Np(\mathcal{V} = n) \end{bmatrix} \\ &= \begin{bmatrix} p(\mathcal{V} = 1) \\ p(\mathcal{V} = 2) \\ \vdots \\ p(\mathcal{V} = n) \end{bmatrix} \\ &= \begin{bmatrix} \pi_k(u' \rightarrow 1) \\ \pi_k(u' \rightarrow 2) \\ \vdots \\ \pi_k(u' \rightarrow n) \end{bmatrix}.\end{aligned}\tag{Eq. 8}$$

If $\mathcal{V} \sim \mathcal{N}_1(u)$, we instead have

$$\mathbb{E}_{\mathcal{V} \sim \mathcal{N}_1(u)}[\text{AGGREGATE}(\mathcal{V})] = \begin{bmatrix} \pi_1(u \rightarrow 1) \\ \pi_1(u \rightarrow 2) \\ \vdots \\ \pi_1(u \rightarrow n) \end{bmatrix}.$$

From Lemma 1 we know that there exists at least one $v \in \mathcal{N}_1(u)$ such that $\pi_1(u \rightarrow v) \neq \pi_k(u' \rightarrow v)$. Therefore, $\mathbb{E}_{\mathcal{V} \sim \mathcal{N}_k(u')}[\text{AGGREGATE}(\mathcal{V})] \neq \mathbb{E}_{\mathcal{V} \sim \mathcal{N}_1(u)}[\text{AGGREGATE}(\mathcal{V})]$, so AGGREGATE($\mathcal{N}_k(u')$) is a biased estimator of AGGREGATE($\mathcal{N}_1(u)$). \square

This result holds for other common aggregators like SUM and MAX for single samples. For MAX, however, the sample size matters, because the expected value for the j^{th} feature is the probability that

j is sampled at least once. We conjecture that this is problematic for larger sample sizes in weighted graphs, and is perhaps the reason why mean-pooling outperformed max-pooling for our GraphSAGE baseline during our initial experiments (Section C).

B Data details

- Air:** Flight trajectories of passenger itineraries in the United States. Nodes represent airport locations (cities) and edges represent passengers flying between locations. The itineraries were retrieved from the Airline Origin and Destination Survey (DB1B) database, which is publicly available through the U.S. Bureau of Transportation Statistics³. We downloaded all records between Jan. 1 and Dec. 31, 2019 from the DB1BCoupon table, joined and sorted itineraries using the "ITIN_ID" and "SEQ_NUM" columns, and discarded any itineraries with missing origin or destination information. Node classes represent the geographical location of each airport, aggregated by standard federal region of the United States. While we extracted this particular set of paths, this database has been utilized in prior work [35].
- T2D:** Disease trajectories for type 2 diabetes patients in the state of Indiana [23]. Nodes represent ICD9 diagnosis codes and edges represent sequential diagnoses. Following prior work, we only preserved the first occurrence of each diagnosis code for each patient; however, we did not split trajectories based on the period of time between diagnoses. Node classes are the chapters of each ICD9 code, which represent categories of disease classification.
- Wiki:** Clickstreams of users playing the Wikispeedia game, in which a player attempts to navigate from a source to a target article by clicking only Wikipedia links [43]. Here, nodes represent Wikipedia articles, and edges represent user clicks between articles. We included both finished and unfinished paths. Node classes are the subjects of each article.
- NY:** Readership trajectories for a large online magazine from Jan 1. to Apr. 15, 2020 [41]. Nodes represent online content (articles, games, etc.), and edges represent sequential clicks by users. We only considered trajectories in which the user visited at least three nodes during a session. Node classes represent the content type (magazine, culture, news, or humor).

³<https://transtats.bts.gov/>. Accessed April 14, 2022.

C Hyperparameter configurations

We manually tuned hyperparameters for each model. Table 4 summarizes the configurations that we evaluated in reporting the main results in Tables 2 and 3. We used the Adam optimizer with a learning rate of 0.0005 for GAT and GATv2, and a learning rate of 0.01 for all other models. For minibatch models (GraphSAGE, GIN, and DGE), we tested batch sizes of 16, 32, and 64. Unless otherwise noted, all results reported in Tables 2, 3, 5, and 6 were the best-performing configuration for each model as averaged across all testing folds.

In general, the most impactful hyperparameter was the number of GNN layers. As discussed in Section 4.2, on Air, T2D, and NY, all baselines performed best with only a single layer for both node classification and link prediction. On Wiki, several models performed best with 3 layers (Figure 3). GCNII, which uses residual connections and is thus designed with deep GNNs in mind [9], was the only model we tested with more than 3 layers. For most models, increasing the number of hidden units per layer above 256 had little to no effect on performance. The exception to this was DGE-pool* on Air, which performed best with 2,048 hidden units (Section 4.3).

Other hyperparameters varied by data set. The number of neighbors sampled ($|\mathcal{N}|$) was very important on the dense graphs (T2D and NY). In all cases, we found that increasing the sample size of the first layer was the most important, so we fixed the sample size at the second layer to 1 (per first-layer sample). Baselines preferred 512 samples for T2D and 256 for NY. DGE preferred 256 samples per base learner (the max that we tested) for T2D and 128 for NY. The same trend held for GraphSAINT’s subgraph sampling, which preferred more roots on graphs that were dense and had more nodes (512 for Air and Wiki, 1024 for T2D, and 2048 for NY).

For neighborhood aggregators, max-pooling was in all cases inferior to mean-pooling and sum-pooling, likely due to the inability of max-pooling to appropriately distinguish dense neighborhoods [46].

Table 4: Hyperparameters evaluated for each model.

Model-specific hyperparameters		
Model	# Layers	Other
GCN	{1, 2, 3}	—
GCNII	{1, 2, 3, 4, 6, 8}	$\alpha = 0.5, \lambda = 1.0$
GAT	{1, 2, 3}	attnheads = {4, 8, 16}
GATv2	{1, 2, 3}	attnheads = {4, 8, 16}
GraphSAGE	{1, 2, 3}	$ \mathcal{N} = \{32, 64, 128, 256, 512, 1024\} \times \{1, 2, 4, 8\} \times \{1\}$ AGGREGATE = {MEANPOOL, MAXPOOL}
GIN	{1, 2, 3}	$ \mathcal{N} = \{32, 64, 128, 256, 512, 1024\} \times \{1, 2, 4, 8\} \times \{1\}$
GraphSAINT	{1, 2, 3}	nroots = {256, 512, 1024, 2048}, walklen = {2, 3, 4}
DGE (all)	{1, 2, 3}	$\ell = \{4, 8, 16\}, \mathcal{N} = \{32, 64, 128, 256\} \times \{1, 2, 4\} \times \{1\}$
General hyperparameters		
Model	Dropout	Hidden units (per layer)
All	0.4	{128, 256, 512, 1024, 2048}

D Additional results

To support our claim that existing GNNs cannot effectively use G_2 as input, we also tested each baseline using G_2 as the input graph. As we expected, because each node in a HON is a fragmented representation of its base node, performance was generally worse (or about the same) when compared to G_1 . Tables 5 and 6 detail the full results. Table 5 also includes results for one additional pooling mechanism, DGE-attn, which pooled representations from the sampled relatives via a self-attention mechanism. Since it did not generalize particularly well in the node classification experiments, we did not discuss it in the main manuscript and did not evaluate its performance on link prediction. More details are available in Appendix E.

Figure 6 shows classifier accuracy and diversity (Section 4.3) for the Wiki and NY data sets, as a supplement to Figure 5.

Table 5: Results from Table 2 (micro F1 on node classification) expanded to include baseline performance when using G_2 as input. Bold font indicates the best result for each data set.

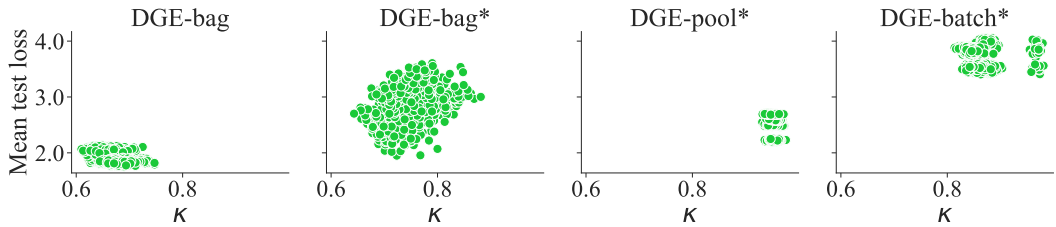
Model	Input	Air	T2D	Wiki	NY
GCN	G_1	0.818 ± 0.03	0.480 ± 0.02	0.643 ± 0.01	0.796 ± 0.01
	G_2	0.805 ± 0.05	0.500 ± 0.02	0.665 ± 0.02	0.744 ± 0.02
GCNII	G_1	0.845 ± 0.05	0.511 ± 0.02	0.654 ± 0.02	0.801 ± 0.01
	G_2	0.833 ± 0.05	0.537 ± 0.03	0.657 ± 0.02	0.816 ± 0.01
GAT	G_1	0.804 ± 0.03	0.282 ± 0.10	0.639 ± 0.02	0.487 ± 0.06
	G_2	0.817 ± 0.05	0.253 ± 0.03	0.646 ± 0.03	0.512 ± 0.04
GATv2	G_1	0.838 ± 0.03	0.292 ± 0.07	0.643 ± 0.03	0.495 ± 0.05
	G_2	0.842 ± 0.05	0.241 ± 0.10	0.646 ± 0.03	0.512 ± 0.13
GraphSAGE	G_1	0.781 ± 0.04	0.654 ± 0.04	0.625 ± 0.02	0.828 ± 0.02
	G_2	0.688 ± 0.02	0.516 ± 0.01	0.633 ± 0.01	0.818 ± 0.01
GIN	G_1	0.745 ± 0.02	0.673 ± 0.04	0.636 ± 0.02	0.826 ± 0.02
	G_2	0.660 ± 0.02	0.637 ± 0.03	0.625 ± 0.02	0.812 ± 0.02
GraphSAINT	G_1	0.802 ± 0.02	0.600 ± 0.07	0.664 ± 0.01	0.821 ± 0.02
	G_2	0.710 ± 0.03	0.567 ± 0.03	0.661 ± 0.02	0.828 ± 0.01
HONEM	G_1, G_2	0.805 ± 0.04	0.566 ± 0.02	0.588 ± 0.01	0.728 ± 0.02
DGE-concat	G_2	0.825 ± 0.04	0.501 ± 0.06	0.615 ± 0.02	0.790 ± 0.02
DGE-concat*	G_2	0.810 ± 0.04	0.439 ± 0.03	0.577 ± 0.02	0.761 ± 0.02
DGE-pool	G_2	0.839 ± 0.03	0.735 ± 0.03	0.671 ± 0.01	0.860 ± 0.01
DGE-pool*	G_2	0.865 ± 0.02	0.555 ± 0.07	0.599 ± 0.04	0.775 ± 0.01
DGE-bag	G_2	0.856 ± 0.02	0.770 ± 0.04	0.681 ± 0.00	0.871 ± 0.01
DGE-bag*	G_2	0.766 ± 0.04	0.719 ± 0.04	0.644 ± 0.02	0.841 ± 0.02
DGE-batch*	G_2	0.764 ± 0.03	0.646 ± 0.01	0.623 ± 0.01	0.818 ± 0.01
DGE-attn	G_2	0.829 ± 0.03	0.549 ± 0.05	0.618 ± 0.02	0.775 ± 0.05

* shared parameters

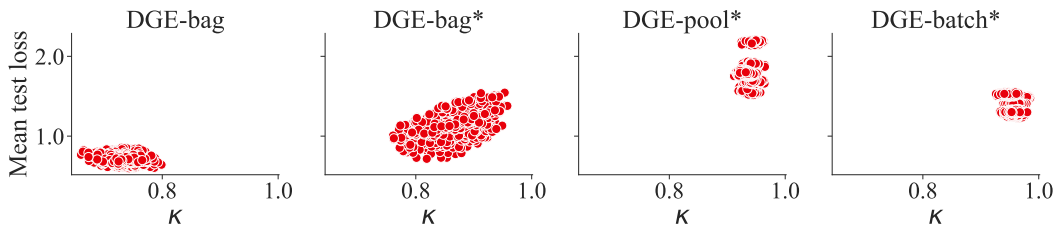
Table 6: Results from Table 3 (AUPRC on link prediction) expanded to include baseline performance when using G_2 as input. Bold font indicates the best result for each data set.

Model	Input	Air	T2D	Wiki	NY
GCN	G_1	0.794 \pm 0.01	0.793 \pm 0.00	0.741 \pm 0.01	0.742 \pm 0.00
	G_2	0.777 \pm 0.02	0.781 \pm 0.00	0.749 \pm 0.01	0.753 \pm 0.00
GCNII	G_1	0.806 \pm 0.01	0.754 \pm 0.01	0.781 \pm 0.01	0.750 \pm 0.00
	G_2	0.771 \pm 0.01	0.732 \pm 0.00	0.790 \pm 0.01	0.759 \pm 0.00
GAT	G_1	0.786 \pm 0.01	0.698 \pm 0.02	0.797 \pm 0.01	0.644 \pm 0.00
	G_2	0.768 \pm 0.01	0.681 \pm 0.01	0.801 \pm 0.01	0.641 \pm 0.00
GATv2	G_1	0.771 \pm 0.01	0.701 \pm 0.01	0.794 \pm 0.01	0.645 \pm 0.01
	G_2	0.784 \pm 0.01	0.684 \pm 0.00	0.796 \pm 0.01	0.660 \pm 0.01
GraphSAGE	G_1	0.782 \pm 0.02	0.713 \pm 0.01	0.758 \pm 0.01	0.717 \pm 0.00
	G_2	0.757 \pm 0.02	0.712 \pm 0.01	0.756 \pm 0.01	0.716 \pm 0.00
GIN	G_1	0.800 \pm 0.01	0.704 \pm 0.00	0.745 \pm 0.01	0.717 \pm 0.00
	G_2	0.748 \pm 0.02	0.702 \pm 0.00	0.743 \pm 0.01	0.716 \pm 0.00
GraphSAINT	G_1	0.718 \pm 0.01	0.797 \pm 0.00	0.688 \pm 0.01	0.750 \pm 0.00
	G_2	0.702 \pm 0.02	0.791 \pm 0.01	0.694 \pm 0.01	0.756 \pm 0.00
HONEM	G_1, G_2	0.697 \pm 0.02	0.818 \pm 0.00	0.589 \pm 0.01	0.769 \pm 0.00
DGE-concat	G_2	0.886 \pm 0.01	0.815 \pm 0.01	0.774 \pm 0.01	0.802 \pm 0.00
DGE-concat*	G_2	0.856 \pm 0.01	0.779 \pm 0.01	0.712 \pm 0.02	0.898 \pm 0.00
DGE-pool	G_2	0.851 \pm 0.02	0.920 \pm 0.00	0.838 \pm 0.03	0.913 \pm 0.00
DGE-pool*	G_2	0.845 \pm 0.01	0.901 \pm 0.00	0.802 \pm 0.06	0.769 \pm 0.01
DGE-bag	G_2	0.887 \pm 0.00	0.907 \pm 0.00	0.876 \pm 0.01	0.921 \pm 0.00
DGE-bag*	G_2	0.862 \pm 0.02	0.894 \pm 0.00	0.856 \pm 0.00	0.916 \pm 0.00
DGE-batch*	G_2	0.853 \pm 0.03	0.871 \pm 0.01	0.830 \pm 0.01	0.887 \pm 0.00

* shared parameters



(a) Wiki results.



(b) NY results.

Figure 6: Mean node classification loss of each pair of classifiers, plotted as a function of Cohen's kappa (lower values indicate lower agreement). Each point represents one pairwise comparison between the 16 classifiers in each of the 5 testing folds. All plots contain the same number of points.

E Additional pooling mechanisms

In addition to Eqs. 5a, 5b, and 5c, we evaluated an attention mechanism (inspired by GAT [40]) which used self-attention to pool the outputs of all sampled relatives. We computed attention coefficients e_{ij} for each $i, j \leq \ell$ according to

$$e_{ij} = F\left(\mathbf{W}(\text{GNN}_i(D_u^{(i)})), \mathbf{W}(\text{GNN}_j(D_u^{(j)}))\right), \quad (10)$$

where F is a single-layer feed-forward network with a LeakyReLU activation, $\mathbf{W} \in \mathbb{R}^{2d \times d}$ is a trainable weight matrix, and $\text{GNN}_i(u) = \mathbf{h}_u^{(i,t)}$ (as in Eqs. 5a and 5b). We then computed the final attention coefficients α_{ij} according to

$$\alpha_{ij} = \text{softmax}_i(e_{ij}) = \frac{\exp(e_{ij})}{\sum_{m=1}^{\ell} \exp(e_{im})}. \quad (11)$$

We repeated this procedure for K separate attention heads. Whereas the original GAT layer averages the outputs of the attention heads before applying a non-linear activation [40], we found that passing the same output to another feed-forward network provided better results. Formally, letting i be the index of we compute the vector of class probabilities $\hat{\mathbf{y}}_u$ by

$$\hat{\mathbf{y}}_u = \sigma\left(F'\left(\sigma'\left(\frac{1}{K} \sum_{n=1}^K \left\| \sum_{j=1}^{\ell} \alpha_{ij}^{(n)} \mathbf{W}^{(n)} \text{GNN}_j(D_u^{(j)}) \right\| \right)\right)\right) \quad (12)$$

where $\|$ is vector concatenation, F' is a feed-forward network with output dimension $d/4$ (followed by batch normalization and a LeakyReLU activation), $\alpha_{ij}^{(n)}$ and $\mathbf{W}^{(n)}$ represent the attention coefficients and linear transformation, respectively, for the n^{th} attention head, and σ' is a LeakyReLU activation. For our experiments, we set $K = 5$, $d = 128$, and a negative slope coefficient of 0.3 for all LeakyReLU activations. We refer to this model as DGE-attn and discuss its performance in Appendix D.

F Ensemble size

Due to the efficiency and scalability issues inherent to ensemble methods, we evaluated two additional questions:

1. How many base learners (ℓ) does DGE require?
2. Can we reproduce similar results with weak (i.e., low parameter cost) base learners?

Figure 7 shows that the optimal number of base learners varied from 4 (NY) to 12 (Air and T2D). On Air and T2D the models using weak base learners—which used about 10% of the number of parameters (e.g., Air used 7.1k parameters for each weak base learner and 71k for each strong base learner)—performed notably worse. However, on Wiki and NY, the weak base learners performed about the same.

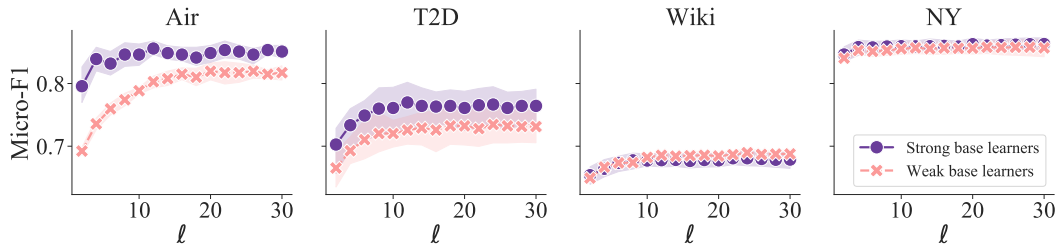


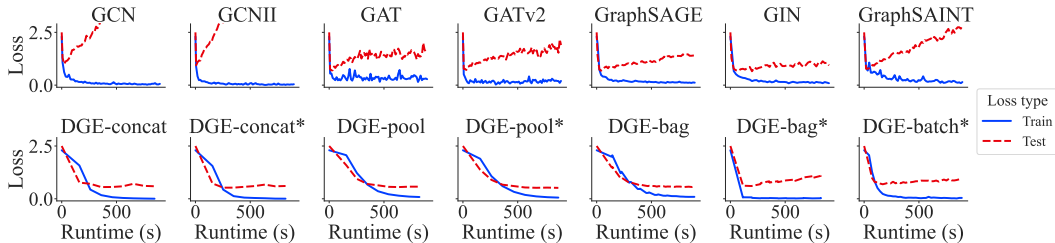
Figure 7: Node classification performance of DGE-bag (2 layers) as a function of the number of base learners. The strong base learners each had 128 hidden units per layer and weak base learners had 16 hidden units. Shaded areas represent standard deviation across testing folds.

G Training time and convergence

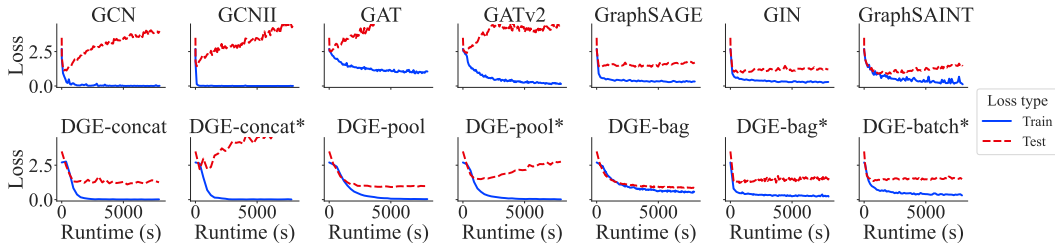
We analyzed the additional time cost incurred by DGE by plotting training and testing loss as a function of total runtime for Air and T2D. We used an NVIDIA GeForce GTX TITAN X GPU and dual 8-core 2.4GHz Intel Xeon processors for each model. As Figure 8 shows, DGE generalized significantly better than all baselines. While the baselines typically converged quickly on the training set, they also rapidly began to overfit on the testing set. The increase in test error was sharper for the full-batch models like GCN and GCNII since they completed more epochs in a shorter period of time. DGE-bag, and, to a lesser extent, DGE-pool, generalized extremely well. These observations reflect overall model performance as reported in Table 2. One difference is that many of the baseline results reported in Table 2 used only a single GNN layer (Section 4.2). For the results in Figure 8, we fixed the number of GNN layers to 2 in order to confirm that the poor generalization of baselines (Section 4.2) was not due to lack of model capacity or underfitting the training set. This is why some models, like GCNII on Air, were relatively competitive in the main results but show high generalization error here.

The sample-based methods, including DGE, incurred significant overhead from neighbor sampling (over 95% of total runtime). This was exacerbated by the fact that all models preferred a high number of neighbor samples at the first layer, so repeatedly sampling a single neighbor at the second layer (Appendix C) produced substantial procedural overhead. DGE would train significantly faster with a more efficient mechanism for sampling these two-hop neighbors (such as pre-fetching).

Finally, we note that the time complexity of DGE scales linearly with the complexity of the base GNN, since we are essentially constructing ℓ copies of that GNN (or, in the case of shared parameters, repeating ℓ forward passes per example). The time incurred by relative resampling via Eq. 3 ($O(\ell|V|)$) and pooling via Eqs. 5a, 5b, and 5c, is trivial compared to the complexity of Eq. 2.



(a) Air results.



(b) T2D results.

Figure 8: Node classification loss for 2-layer models on the first testing fold, shown as a function of training time. Runtime is measured as wallclock time from the start of the first epoch. High loss values are truncated to preserve scale. Similar trends held for all testing folds.

H Analysis of node characteristics

To better understand DGE’s performance, we analyzed the node classification predictions by plotting the change in test loss for each node (Figure 9). We hypothesized that DGE would provide the strongest improvements on nodes with higher out-degree and larger higher-order families ($|\Omega^2|$); however, this was not consistently true for all data sets. Instead, we found that a node’s homophily (\mathcal{H} , defined as the fraction of neighbors that have the same class) was the best predictor of performance improvement. This observation is noteworthy for future work, especially since most GNNs struggle to model graphs with low homophily [51].

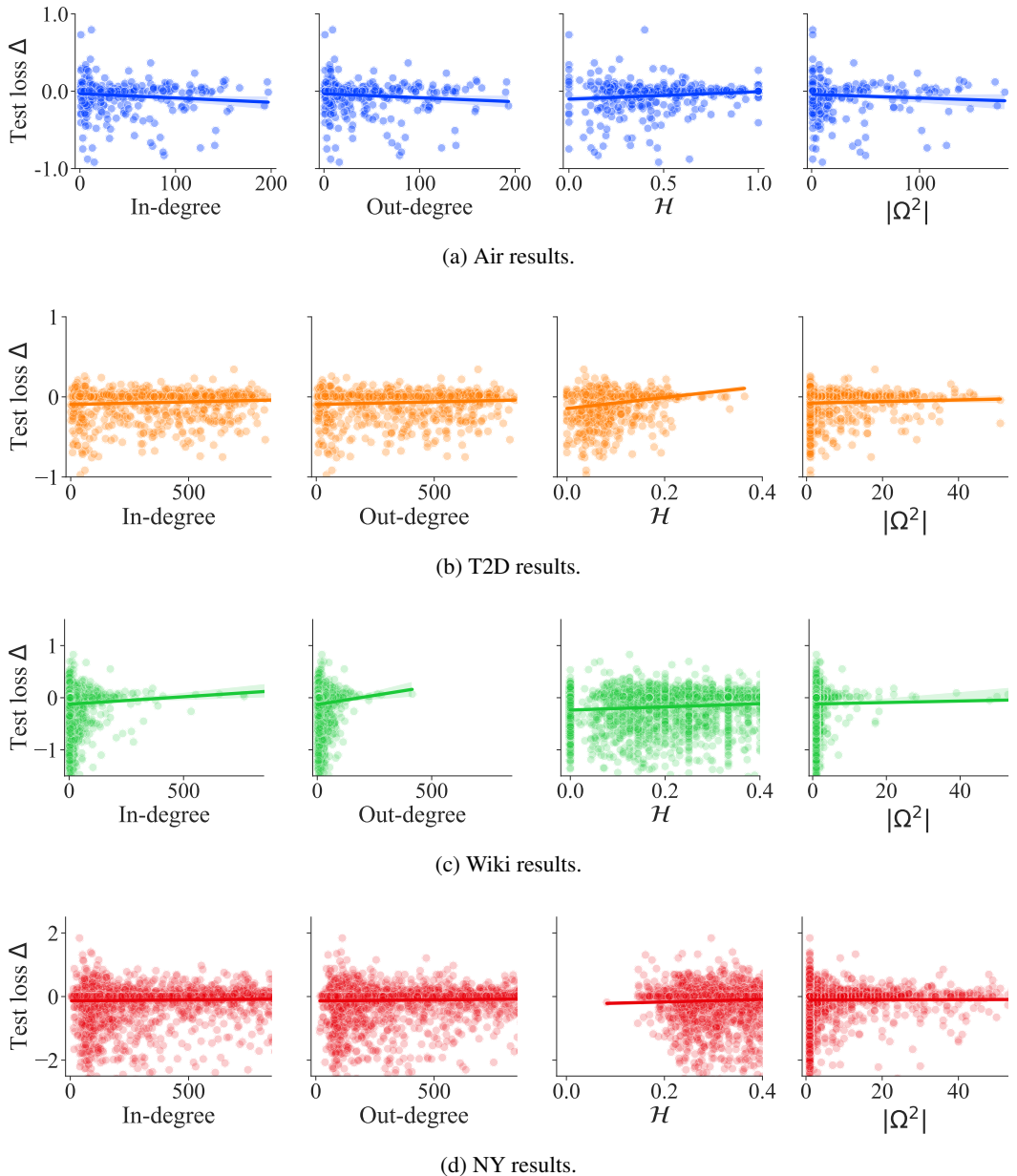


Figure 9: Delta in test loss for DGE-bag compared to GraphSAGE (the base GNN) for node classification (i.e., values < 0 mean that GraphSAGE produced higher loss than DGE-bag), plotted as a function of key node features in G_1 . Out-degree and in-degree are unweighted. Each point represents a node in the test set. All five testing folds are included. Shading represents the 95% CI for the regression line.

I Higher-order network construction

We used GrowHON [22] to construct all HONs. GrowHON provides a parameter τ which helps control the size and fit of the graph by raising the KL-divergence threshold required for a new higher-order node to be created, and we found that the choice of τ impacted DGE’s success in each task. Figure 10 shows the results of varying τ for each data set and task. In general, the optimal τ value varied between data sets for classification tasks, while for link prediction, a lower τ generally yielded better results. We did not tune DGE’s hyperparameters for these experiments, so it is likely that further tuning would reduce the difference between each model. However, these observations have important consequences for future work, especially with respect to integrating prior studies on graph structure learning, which have argued that different graph representations may be useful for different predictive tasks [8]. Ideally, we could incorporate HON construction into the learning framework so that the model could learn the structure that is best-suited to each task.

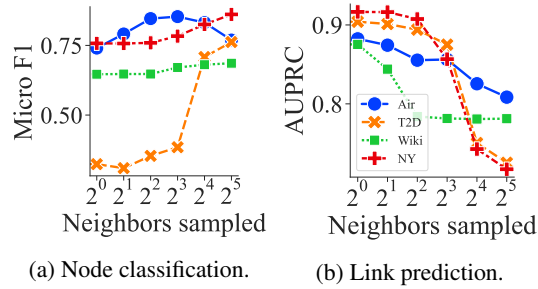


Figure 10: Performance as a function of τ . Each point represents the mean of all 5 testing folds.